ISBN: 978-3-95450-261-5 ISSN: 2673-7000 doi: 10.18429/JACoW-NAPAC2025-TUP086

SIMULATIONS OF CSR AND LSC INDUCED MICROBUNCHING IN THE PRESENCE OF A LASER HEATER*

S. Kladov†, Y.-K. Kim, University of Chicago, Chicago, IL, USA
C. Emma, Z. Huang, S. Gessner, SLAC National Accelerator Laboratory, Menlo Park, CA, USA

Abstract

We present a study of microbunching instability in the FACET-II linac, in which the amplification and damping mechanisms are analyzed separately. Our simulations investigate the gain induced by Longitudinal Space Charge (LSC) and, critically, the damping caused by nonlinear terms in the beam transport transfer map. We show theoretically and through simulation that these nonlinear effects can produce damping several orders of magnitude stronger than predicted by linear theory.

Experimental evidence validates these findings. A quadrupole scan performed in the FACET-II dogleg reveals that an interaction between coherent betatron oscillations and transfer map nonlinearities shifts the point of minimal damping away from the expected linear condition of $R_{51} = 0$. The strong agreement between our simulations and the experimental data demonstrate that a thorough understanding of nonlinear dynamics is essential for high-brightness beam transport.

INTRODUCTION

Microbunching is defined as density modulations within a particle beam. Controlling and understanding the dynamics of the phenomenon is increasingly critical, as modern accelerator applications impose stringent limits on the amplitude of such modulations, particularly at short wavelengths. For example, Coherent Electron Cooling at the future Electron-Ion Collider [1] requires that modulations in the electron beam remain only slightly above the shot-noise level at wavelengths smaller than 10 µm [2–4]. Furthermore, for beams at moderate energies (300 MeV for electrons) with a transverse rms size smaller than 1 mm, the Space Charge (SC) impedance – a primary driver of the instability – shifts into the Near-Infrared (NIR) region (< 10 µm).

It is convenient to study the density modulations in the Fourier domain. The Fourier spectrum of the longitudinal distribution of the bunch is called "bunching factor" b [5]:

$$b(k) = \frac{1}{N}\sum_{j=1}^{N} \exp\left(-i\,k\,z_j\right), \tag{1}$$

where z_j is the position of the j particle at a given time, $k = 2\,\pi/\lambda$ is the wavenumber, and N is the total number of particles in the bunch.

The microbunching dynamics can be split into two parts: Gain and Damping. First, we will examine the Gain part induced by SC and CSR.

* Work supported by USDOE, Office of Science AC02-76SF00515.
† kladov@uchicago.edu

SC AND CSR INDUCED GAIN

The theoretical treatment of LSC-induced microbunching gain conceptually divides the lattice into sections: a "gain" section where SC induces an energy modulation, followed by an "R_{56}" section where this energy modulation is converted into a density modulation. For a system with multiple chicanes, the total gain is the product of the gains from each section.

The process begins with initial density modulations, $\Delta\rho(k)$, which may arise from sources such as imperfections at the cathode. These density fluctuations drive a proportional energy modulation, $\Delta\delta(k)$, where $\delta = (\gamma - \gamma_0)/\gamma_0$ is the relative energy deviation of a particle with relativistic factor γ from a reference particle with γ_0. The subsequent R_{56} section, typically a bunching chicane, then transforms this energy modulation into a longitudinal position shift via the linear transfer matrix element: $\Delta z = R_{56}\,\Delta\delta$. Consequently, the final bunching factor, $b_f(k_f)$, is proportional to the initial one, $b_0(k)$, such that $|b_f(k_f)| = |b_0(k)|\,G$. Here, G is the gain and k_f is the final wavenumber, accounting for the overall bunch compression. The Longitudinal SC (LSC) induced gain is well described in [6], and for a small initial modulation amplitude, it takes the form:

$$\begin{aligned} G &\approx \frac{I_0}{\gamma\,I_A}\left|k_f R_{56}\int_0^L \mathrm{d}s\,\frac{4\,\pi\,Z_{\mathrm{LSC}}(k_0;s)}{Z_0}\right| \mathrm{e}^{-\frac{1}{2}k_f^2\,R_{56}^2\,\sigma_{\delta,u}^2}, \\ Z_{\mathrm{LSC}}(k) &= \frac{i\,Z_0}{\pi\,k\,r_b^2}\left[1-\frac{k\,r_b}{\gamma}K_1\left(\frac{k\,r_b}{\gamma}\right)\right], \end{aligned} \tag{2}$$

where I_0 is the peak bunch current, I_A is the Alfven current, L is the length of the gain section (without R_{56}), $Z_{\mathrm{LSC}}(k)$ is the SC impedance, Z_0 is the impedance of free space, r_b is the radius of the bunch (the transverse distribution is assumed uniform cylindrical), and $\sigma_{\delta,u}$ is the initial uncorrelated energy spread. The exponential term in Eq. (2), that represents the conventional damping from an initial uncorrelated energy spread, $\sigma_{\delta,u}$, was added for a clearer relation to the existing theories and comparison with simulations. The factorization of gain and damping is valid because the LSC-induced energy modulation does not depend on a particle's initial energy, as detailed in [7].

A comparison between the conventional SC gain theory and simulations for a section of the FACET-II lattice [8] is presented in Fig. 1. The simulations were performed using BMAD [9], focusing on the relevant lattice section shown in Fig. 2. To adhere to the theoretical assumptions, we analyze only the region from the end of the L1 accelerating section to the end of the BC11 chicane (PR11375). The drift (gain) section has a length of is $L = 0.77$ m, followed by a chicane with $R_{56} = -46$ mm. The bunch has a mean energy of $\gamma_0 = 655$, rms sizes of $\sigma_x = 0.27$ mm, $\sigma_y = 0.36$ mm, a

ISBN: 978-3-95450-261-5 ISSN: 2673-7000 doi: 10.18429/JACoW-NAPAC2025-TUP086

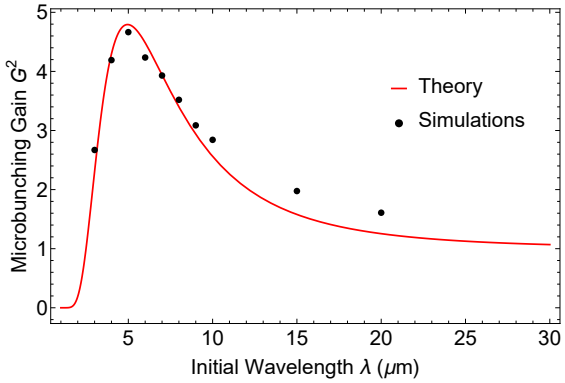

Figure 1: Theory and simulations for the SC-induced microbunching gain in the FACET-II BC11.

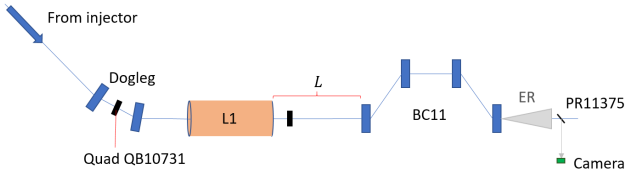

Figure 2: Part of the FACET-II lattice used in the paper. The gain from Fig. 1 corresponds to the BC11 section: from the end of L1 to the end of BC11.

peak current of $I_0 = 207$ A, and the energy spread $\sigma_{\delta,u} = 1.5 \times 10^{-5}$. The initial bunch is gaussian, modulated at a wavelength λ. To suppress the effect of the nonlinear terms of the transfer map T_{5ij}, that will be discussed below, the transverse momenta of the bunch are set to zero, and are reset to zero at the end of the drift section. A small section length was chosen because of a small resolution of the simulations: the initial bunching factor is $|b_0(\lambda)|^2 = 0.05$. Following the theory, the SC in the simulations acts on the bunch only in the drift section, and the dynamics in the chicane is completely single-particle.

In contrast, Coherent Synchrotron Radiation (CSR) generates gain only at the R_{56} sections (in dipoles). CSR also induces an energy modulation proportional to the bunching factor; however, this modulation is simultaneously converted to a density modulation within the same element. Because these processes are coupled, they cannot be split into separate gain and drift sections and require a more complex integral treatment, as described in [10]. Nevertheless, for a qualitative analysis, the damping effects discussed below can still be treated as a factorizable term.

SECOND-ORDER LONGITUDINAL ABERRATIONS WITH MICROBUNCHING

The microbunching damping is caused by effects that alter the density $\Delta\rho(k)$ or $\Delta\delta(k)$ distributions without the proportionality $|b_f(k_f)| \sim |b_0(k)|$. Qualitatively, the damping can be written as

$$G \approx G_0 \exp\left[-k_f^2\, \sigma_{z,\mathrm{ind}}^2\right], \qquad (3)$$

where G_0 is the gain in the absence of damping, and $\sigma_{z,\mathrm{ind}}$ is the uncorrelated longitudinal position spread gained between the start of the gain section and the end of the R_{56} section.

Usually, when the transverse and longitudinal microbunching structures are not correlated, the $\sigma_{z,\mathrm{ind}}$ is induced by the uncorrelated spreads at the beginning of the gain section through the linear and nonlinear transfer map terms R_{5i} and T_{5ij}, $i,j \neq 5$. The damping effect by some of the linear terms is well studied [7], where other linear terms can be easily included.

Here we assumed that the damping is described by a separate multiplier, which is straightforward to see when it is caused by the momenta spread (p_x, p_y, δ), and can be used as an approximation for the terms containing x and y when the transverse size of the bunch is small enough: $k\,\sigma_x \gg \gamma_0$ [7].

The spread can also be induced by correlated modulations, such as from a laser heater [6], but at the wavelength outside of the gain curve. For instance, the FACET-II laser heater introduces approximately $\sigma_{z,\mathrm{ind}} \approx 0.3$ mm for the BC11 chicane gain section [8].

The nonlinear terms in the transfer map add up to the spread $\sigma_{z,\mathrm{ind}}$, resulting in stronger microbunching damping. The main source of these terms is the nonlinear path length dependence (specifically the terms T_{522} and T_{544}) in a drift. Indeed, the drift map is written as

$$c\,\Delta t = c\,L\left[\frac{1}{v_z} - \frac{1}{v_{z,0}}\right] \approx L\left[-\frac{\delta}{\gamma_0^2} + \frac{p_\perp^2}{2} + \frac{3\,\delta^2}{2\,\gamma_0^2}\right], \qquad (4)$$

where v_z is the longitudinal velocity of the particle, $v_{z,0}$ is the longitudinal velocity of the reference particle, and $p_\perp = \sqrt{p_x^2 + p_y^2} = v_\perp / v_z$ is the transverse momentum in radians (p_x and p_y are also in radians). The terms T_{511} and T_{533} originate from magnetic elements such as quadrupoles, where momentum is changed based on x and y: $\Delta p_x = -k\,x$.

The effect strength is different at different parts of the lattice. At the FACET injector (with the injector chicane), the nonlinear terms result in the induced spread of $\sigma_{z,\mathrm{ind}} \sim 10\,\mu$m, that damps the gain completely. We will study the second section, with another chicane BC11, where the induced spread is only of the order of $\sigma_{z,\mathrm{ind}} \sim 1\,\mu$m.

EXPERIMENT

To verify the effect of the first and second order terms, an experiment was conducted. The experiment is a quadrupole scan in the dogleg, that is shown in Fig. 2. The signal used in the analysis is the signal from a CCD camera at the location "PR11375" at the exit of the last dipole of the BC11 chicane.

The signal at the camera is approximately a convolution of the sum of Edge Radiation (ER), Synchrotron Radiation (SR), and Transition Radiation (TR) with the responsivity of the camera $R(\lambda)$:

$$I = \int \left[\frac{\mathrm{d}W_{\mathrm{ER}}}{\mathrm{d}\lambda} + \frac{\mathrm{d}W_{\mathrm{SR}}}{\mathrm{d}\lambda} + \frac{\mathrm{d}W_{\mathrm{TR}}}{\mathrm{d}\lambda}\right] R(\lambda)\,\mathrm{d}\lambda. \qquad (5)$$

The induced longitudinal spread due to the initial uncorrelated energy spread $\sigma_{\delta,u}$ is $\sigma_{z,\mathrm{ind}} = R_{56}\,\sigma_{\delta,u} \approx 0.7\,\mu$m.

ISBN: 978-3-95450-261-5 ISSN: 2673-7000 doi: 10.18429/JACoW-NAPAC2025-TUP086

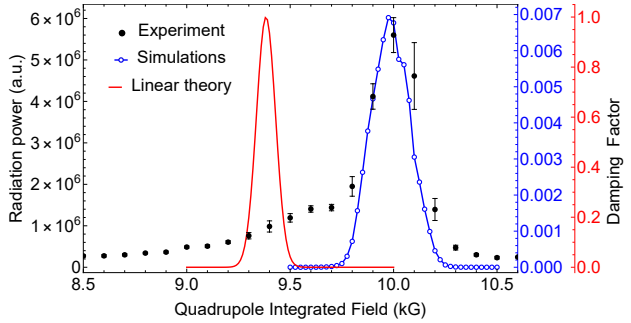

Figure 3: Experimentally observed Coherent Radiation (CSR, CER, TR) (black). Its comparison with the damping factor from the linear theory (red) and simulations (blue) with no uncorrelated energy spread and $\lambda_0 = 2\,\mu$m initial modulation wavelength. The abscissa is the field in the dogleg quadrupole, introducing the linear term R_{51}. The effect of the nonlinear terms is visible in the shift of the peak from the $R_{51} = 0$ location.

According to Eq. (2), any microbunching with the final wavelength $\lambda_f \ll 2\,\pi\,0.7 = 4.4\,\mu$m is damped. The compression ratio in the chosen section is 2, while the camera responsivity cutoff is at around 1 µm. Summing everything up, and taking into account that all the radiation types have the same dependence on the bunching factor: $\frac{dW}{d\lambda} \sim |b_f(\lambda)|^2$, it can be safely assumed that the signal on the camera is proportional to $|b_f(\lambda_0 = 2\,\mu\text{m})|^2$, where λ_0 is the initial modulation wavelength.

The dogleg introduces the R_{51} term, scaling linearly with the quadrupole focusing strength K:

$$R_{51} = a\,(K - K_0), \tag{6}$$

where a is some constant. For the FACET dogleg, the quadrupole detuning of the integrated field by 0.1 kG results in $R_{51} \approx 6 \times 10^{-3}$, and hence, the $\sigma_{z,\text{ind}} \sim 1\,\mu$m.

BMAD **simulations** were constructed to verify the simultaneous action of R_{51} and nonlinear terms. The simulation replicates the part of the FACET-II lattice used in the experiment. We simulate only the damping part: the initial modulation amplitude is 1 (the particle density in the nodes is zero), collective effects are turned off. Additionally, the uncorrelated energy spread is turned off because its effect does not depend on K.

A comparison between the experiment, linear theory, and simulations is presented in Fig. 3. The black dots are the experiment results, the blue curve is the simulations, and the red curve is the linear theory. The simulations and the theory are presented for the $\lambda_0 = 2\,\mu$m initial modulation wavelength.

Even though the widths of the damping factor curves from the linear theory and the simulations are approximately the same, the scale is different by several orders of magnitude. The reason is that the linear terms R_{51} and R_{52} change considerably around the $R_{51} = 0$ location, but the nonlinear terms do not. Therefore, nonlinear terms contribute almost constant damping at these quadrupole strength values, which is not taken into account in the linear theory.

The experiment and simulations give a good agreement in terms of the peak width and position. The linear theory gives a peak at the $R_{51} = 0$ location, that is shifted from what observed experimentally. The reason is the coherent betatron oscillations of the bunch. Indeed, the dependence on x of the change in the longitudinal coordinate is given by

$$\Delta z = a\,(K - K_0)\,x + b\,K^2\,x^2, \tag{7}$$

where $a\,(K - K_0) = R_{51}$, $b\,K^2 = T_{511}$, and x is the initial transverse coordinate. We can see that changing K effectively shifts the parabola of the $z(x)$ dependence. The minimal induced spread is reached when the vertex of the parabola $z(x)$ is at the center of the bunch distribution. Therefore, if the bunch is misaligned by $x_0 = \frac{a\,(K_0 - K)}{2\,b\,K^2}$ at the entrance to the dogleg, the induced spread is minimal, and hence, the damping is minimal as well. The experimentally observed shift of the peak from the integrated field of 9.3 kG to 10 kG can be explained by $x_0 \approx 9$ mm. This is only an estimation because only one quadrupole is taken into account, instead of multiple of them present in the real lattice. For instance, the simulations have coherent x oscillations as well, with maximum amplitude of $x_{\max} \approx 5$ mm.

SUMMARY AND DISCUSSION

In this paper, we emphasized the importance of the nonlinear transfer map terms in the computation of the microbunching damping at small wavelengths. We compared the linear theory with nonlinear single-particle simulations, showing that the effect can easily be several orders of magnitude. We verified the simulations by showing an agreement between its linear linear part with the Space Charge induced gain expected from a section with a bunching chicane at FACET-II.

Additionally, a dogleg quadrupole scan was performed to get an experimental support of the obtained results. The simulations of the microbunching damping with the nonlinear terms gave a good agreement with the radiation power observed experimentally. Speciffically, the peak width and location explained by the coherent betatron oscillations interacting with the simultaneous action of the first and second order terms in the transfer map.

ACKNOWLEDGEMENTS

This work was supported by the U.S. Department of Energy under DOE Contract No. DE-AC02-76SF00515.

REFERENCES

[1] F. Willeke and J. Beebe-Wang, "Electron ion collider conceptual design report 2021", Brookhaven National Laboratory (BNL), Tech. Rep. BNL-221006–2021-FORE, 2021. doi:10.2172/1765663

ISBN: 978-3-95450-261-5 ISSN: 2673-7000 doi: 10.18429/JACoW-NAPAC2025-TUP086

[2] G. Stupakov and P. Baxevanis, "Microbunched electron cooling with amplification cascades", *Phys. Rev. Accel. Beams*, vol. 22, no. 3, p. 034 401, 2019. doi:10.1103/PhysRevAccelBeams.22.034401

[3] W. F. Bergan, "Electron diffusion in microbunched electron cooling", *Phys. Rev. Accel. Beams*, vol. 27, no. 8, p. 084 402, 2024. doi:10.1103/PhysRevAccelBeams.27.084402

[4] S. Kladov *et al.*, "Near-infrared noise in intense electron bunches", *arXiv*, 2025. doi:10.48550/arXiv.2412.13482

[5] D. Ratner, "Much ado about microbunching: Coherent bunching in high brightness electron beams", Ph.D. dissertation, 2011. doi:10.2172/1043865

[6] Z. Huang *et al.*, "Suppression of microbunching instability in the linac coherent light source", *Phys. Rev. Spec. Top. Accel. Beams*, vol. 7, no. 7, p. 074 401, 2004. doi:10.1103/PhysRevSTAB.7.074401

[7] D. Ratner, A. Chao, and Z. Huang, "Three-dimensional analysis of longitudinal space charge microbunching starting from shot noise", in *Proc. FEL'08*, Gyeongju, Korea, paper TUPPH041, pp. 338–341, 2008.

[8] SLAC Site Office, "Technical design report for the FACET-II project at SLAC National Accelerator Laboratory", SLAC National Accelerator Lab., Tech. Rep. SLAC-R–1072, 2016. doi:10.2172/1340171

[9] D. Sagan, "Bmad: A relativistic charged particle simulation library", *Nucl. Instrum. Methods Phys. Res. A*, vol. 558, no. 1, pp. 356–359, 2006. doi:10.1016/j.nima.2005.11.001

[10] Z. Huang and K.-J. Kim, "Formulas for coherent synchrotron radiation microbunching in a bunch compressor chicane", *Phys. Rev. Spec. Top. Accel. Beams*, vol. 5, no. 7, p. 074 401, 2002. doi:10.1103/PhysRevSTAB.5.074401